Ultra-Fast Frequency Response of Converter-Dominant Grids Using PMUs

Preprint

Hugo N. Villegas Pico[1] and Vahan Gevorgian[2]

[1] *Iowa State University*
[2] *National Renewable Energy Laboratory*

Presented at the 2019 Wind Integration Workshop
Dublin, Ireland
October 16–18, 2019

NREL is a national laboratory of the U.S. Department of Energy
Office of Energy Efficiency & Renewable Energy
Operated by the Alliance for Sustainable Energy, LLC

This report is available at no cost from the National Renewable Energy Laboratory (NREL) at www.nrel.gov/publications.

Contract No. DE-AC36-08GO28308

Conference Paper
NREL/CP-5D00-75042
January 2020

Ultra-Fast Frequency Response of Converter-Dominant Grids Using PMUs

Preprint

Hugo N. Villegas Pico[1] and Vahan Gevorgian[2]

[1] *Iowa State University*
[2] *National Renewable Energy Laboratory*

Suggested Citation
Villegas Pico, Hugo N and Vahan Gevorgian. 2020. *Ultra-Fast Frequency Response of Converter-Dominant Grids Using PMUs: Preprint*. Golden, CO: National Renewable Energy Laboratory. NREL/CP-5D00-75042. https://www.nrel.gov/docs/fy20osti/75042.pdf.

NREL is a national laboratory of the U.S. Department of Energy
Office of Energy Efficiency & Renewable Energy
Operated by the Alliance for Sustainable Energy, LLC

This report is available at no cost from the National Renewable Energy Laboratory (NREL) at www.nrel.gov/publications.

Contract No. DE-AC36-08GO28308

Conference Paper
NREL/CP-5D00-75042
January 2020

National Renewable Energy Laboratory
15013 Denver West Parkway
Golden, CO 80401
303-275-3000 • www.nrel.gov

NOTICE

This work was authored in part by the National Renewable Energy Laboratory, operated by Alliance for Sustainable Energy, LLC, for the U.S. Department of Energy (DOE) under Contract No. DE-AC36-08GO28308. Funding provided by U.S. Department of Energy Wind Energy Technologies Office. The views expressed herein do not necessarily represent the views of the DOE or the U.S. Government. The U.S. Government retains and the publisher, by accepting the article for publication, acknowledges that the U.S. Government retains a nonexclusive, paid-up, irrevocable, worldwide license to publish or reproduce the published form of this work, or allow others to do so, for U.S. Government purposes.

Cover Photos by Dennis Schroeder: (clockwise, left to right) NREL 51934, NREL 45897, NREL 42160, NREL 45891, NREL 48097, NREL 46526.

Ultra-Fast Frequency Response of Converter-Dominant Grids Using PMUs

Hugo N. Villegas Pico
Department of Electrical and Computer Engineering
Iowa State University
Ames, IA 50011, USA
e-mail: hvillega@iastate.edu

Vahan Gevorgian
National Wind Technology Center
National Renewable Energy Laboratory
Boulder, CO 80303, USA
e-mail: vahan.gevorgian@nrel.gov

***Abstract*—The incorporation of converter-based power sources can act as a substitute for synchronous-machine based generators in an electric power grid. Because power converters are not intrinsically sensitive to frequency transients, the frequency response of these grids might deteriorate. To lessen large frequency excursions, this paper proposes a method to counteract load-generation imbalances by commanding ultra-fast frequency responding converter-based assets such as wind and battery energy storage. The set-points derive from the amount of the imbalance, which is estimated using phasor measurement units (PMUs). Because the proposed technique depends on communications networks, local converter frequency control using an aggressive frequency droop function is also proposed in order to mitigate negative impacts by communications failures and/or cyberattacks. The benefits of the technique are demonstrated on a modified version of the IEEE 39-bus test power system, which incorporates optimally located PMUs as well as wind, solar, and battery energy storage assets. The paper showcases that the proposed developments are instrumental to maintaining frequency close to nominal during relatively large load-generation imbalances and cyberattacks.**

I. Introduction

The progressive incorporation of renewable assets is displacing synchronous generation, which introduces significant challenges to maintaining the frequency response of power systems around the world [1]–[3]. In North America, for example, 72 GW of conventional generation capacity has been retired during the past 10 years, whereas 95 GW and 22 GW of wind and solar generation technologies have been incorporated, respectively [4, p. 50]. The integration of converter-based generation is conceived as problematic for frequency regulation because: (i) their controls are naturally insensitive to load-generation imbalances and (ii) the ratio of synchronously spinning inertia of an electric grid with respect to its total capacity is significantly reduced [1], [3].

At present, available converter control strategies to quickly arrest changes in frequency resort to measuring the frequency's magnitude and its rate of change [5]–[8]. Hence, these regulators can emulate synthetic inertia and droop response via wind power plants (WPP), battery energy storage (BES), solar power plants (SPP), and pumping stations (PPS)—the latter when equipped with variable-frequency drives (VFDs) [9]. Nonetheless, a problem of these controls is that they still depend on the external response of spinning synchronous generators to operate because their action relies on the frequency that is set by rotatory machinery. Thus, the potential for converters to immediately compensate imbalances is not fully exploited.

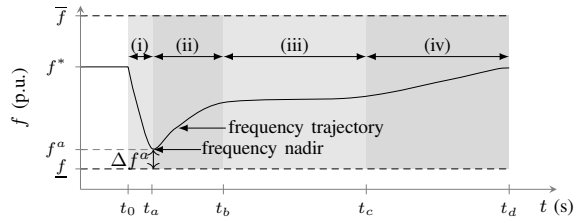

Fig. 1. Frequency trajectory $f(t)$ for $t \in (t_0, t_d]$ [1], [9].

An alternative method to achieve faster compensation to load-generation imbalances resorts to detecting the amount of a disturbance that triggers a frequency transient [3], [10]. If the load-generation imbalance is timely detected, then assets such as the WPP, BES, SPP, and PPS can be commanded to act in an ultra-fast manner (e.g., with respect to the dynamic response of conventional machines) to compensate for the disturbance. To this end, this paper elaborates on estimating load-generation imbalances at any bus of a power system and developing a control strategy to deploy ultra-fast frequency response (ultra-FFR) converter-based assets. The objective is to prevent relatively large off-nominal frequency transients by counteracting the impact of sudden imbalances on an electric grid.

The developments of this paper are significant to reduce the risk associated with under-frequency excursions, which is measured via the margin $\Delta f^a = f^a - \underline{f}$, as shown in Fig. 1 [9]. There, $f^a = f(t_a)$ is the minimum attained frequency or frequency nadir during a frequency transient event, whereas $\underline{f}$ is the under-frequency load shedding (UFLS) threshold. If $f(t)$ falls below the UFLS limit, the load can be disconnected, which harms the reliability of a grid [1], [4]. Note in Fig. 1 that Δf_a is indicative of how close the execution of under-frequency load shedding (UFLS) is; hence, $\Delta f_a \leq 0$ is undesirable [1, p. 113].

In this paper, we consider an optimal number of phasor mesurement units (PMUs) throughout a network that are

This work was authored by Alliance for Sustainable Energy, LLC, the Manager and Operator of the National Renewable Energy Laboratory for the U.S. Department of Energy (DOE) under Contract No. DE-AC36-08GO28308. Funding provided by the the U.S. Department of Energy's Wind Energy Technologies Office (WETO). The views expressed in the article do not necessarily represent the views of the DOE or the U.S. Government. The U.S. Government retains and the publisher, by accepting the article for publication, acknowledges that the U.S. Government retains a nonexclusive, paid-up, irrevocable, worldwide license to publish or reproduce the published form of this work, or allow others to do so, for U.S. Government purposes.

placed at select buses. This is different from the approach in [3], which considered PMUs located only at select generator buses. In our approach, positive-sequence voltages and currents in the network are observed or estimated in order to determine variations of net power injections at each bus of the grid. The causal load-generation imbalance is determined by employing a set of wash-out filters, which extract temporal variations of the power injections at any bus. In addition, we propose an aggressive droop function to back up the proposed ultra-FFR method in case of communications unavailability and/or cyberattacks. For example, stealthy PMU data corruption to provoke erroneous estimations of load-generation imbalances [11]. Thus, a cyberattack can trigger an unnecessary injection of power and cause an overfrequency event, for example.

The remainder of this paper is organized as follows. Section II presents preliminaries pertaining to modeling of transmission lines and PMU placement. Section III introduces details on the detection of load-generation imbalances as well as the disturbance mitigation. Section IV illustrates case studies on a modified IEEE 39-bus power system to show the advantages of the developments within a high-fidelity simulation environment.

II. Preliminaries

A. Transmission Lines and Phasor Measurements

A fundamental application of PMUs consists of estimating phasor representations of voltages and currents at the terminals of a transmission line [12]–[14], e.g., in the proximity to buses b_i and b_j in Fig. 2. A PMU can produce, via signal processing techniques, positive-sequence voltage and current phasors $\tilde{V}_i$ and $\tilde{I}_{k,i}$ that are representative of three-phase quantities close to bus b_i. Note in Fig. 2 that waveform measurements of a transmission line, l_k, are achieved via appropriate instrumentation, e.g., voltage (VT) and current (CT) transformers.[1] Also, the current, $\tilde{I}_j$, for example, models a bus net current injection as a result of several generators and/or loads connected to b_j.

In this paper, the line l_k of Fig. 2 is modeled by a positive-sequence lumped parametric circuit, where R_k, X_k, and B_k represent resistance, reactance, and susceptance, respectively.[2] Using the PMU processed phasors, $\tilde{V}_i$ and $\tilde{I}_{k,i}$, positive-sequence quantities close to bus b_j are estimated:

$$\tilde{V}_j = \tilde{V}_i - (R_k + \mathrm{j}X_k)\tilde{I}_k \tag{1}$$

$$\tilde{I}_{k,j} = -\tilde{I}_k + \mathrm{j}(B_k/2)\tilde{V}_j \tag{2}$$

$$\tilde{I}_k = \tilde{I}_{k,i} - \mathrm{j}(B_k/2)\tilde{V}_i\,. \tag{3}$$

Note in Fig. 2 that $\tilde{I}_{k,i}$ and $\tilde{I}_{k,j}$ are both assumed to leave buses b_i and b_j, respectively. Depending on the placement of the PMUs, $\tilde{V}_i$ and $\tilde{V}_j$ might be available by direct measurement or estimation but not the currents $\tilde{I}_{k,i}$ and $\tilde{I}_{k,j}$. For example, some PMUs might measure currents of contiguous transmission lines that share the bus ends of the k-th one in Fig. 2. In such a case, $\tilde{I}_{k,i}$ and $\tilde{I}_{k,j}$ can also be estimated via (1)–(3).

[1]Instrumentation errors are neglected because they can be mitigated via model-based correction algorithms [15, p. 13].

[2]This representation is a modest approximation of more detailed physical models [16, p. 10].

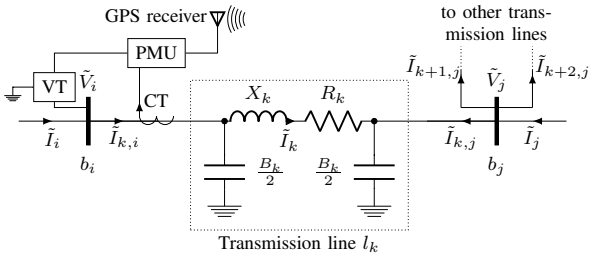

Fig. 2. Lumped-parameter representation of a transmission line for sinusoidal voltages and currents. The arrow of the current transformer specifies instantaneous current direction with respect to that in the transmission line.

These relatively simple applications are instrumental in Section III to *detect* sudden load-generation disturbances throughout a bulk transmission system.

B. Bulk Transmission System and PMU Placement

The bulk transmission system is represented by a set of N buses, $\mathcal{B} = \{b_1, \ldots, b_i, \ldots, b_j, \ldots, b_N\}$, and a collection of M transmission lines, $\mathcal{L} = \{l_1, \ldots, l_k, \ldots, l_M\}$ [17]. Notably, an l_k transmission line, as the one in Fig. 2, is associated with a unique pair of buses, i.e., $l_k \sim \mathcal{L}_k = \{b_i, b_j\} \subseteq \mathcal{B}$, $i \neq j$, signifying that l_k connects buses b_i and b_j. We consider that all buses are *connected*, i.e., there exists a set of contiguous transmission lines that link all possible pairs of buses from $\mathcal{B}$. Further, we assume that the network topology is *invariant* during the study, i.e., there are not transmission line outages.

The connectivity of the transmission system is modeled via a nonoriented incidence matrix, $A \in \{0,1\}^{N\times M}$, where the entries of A are:

$$A_{jk} = \begin{cases} 1 & \text{if } b_j \in \mathcal{L}_k \\ 0 & \text{otherwise} \end{cases} \tag{4}$$

for all $j \in \{1, \ldots, N\}$ and $k \in \{1, \ldots, M\}$. The matrix A is advantageous to place a minimum number of PMUs throughout the transmission network while ensuring that the voltage phasors at each bus b_j can be observed and/or estimated via (1)–(3).

PMUs are placed according to the solution of the following integer programing problem [18]:

$$\begin{aligned} \underset{x_1,\ldots,x_k,\ldots,x_M}{\text{min.}} \quad & \sum_{k=1}^{M} x_k \\ \text{subject to} \quad & Ax \succeq \mathbf{1} \\ & x_k \in \{0,1\},\ k = 1, \ldots, M \end{aligned} \tag{5}$$

with $\mathbf{1}$ an N-dimensional vector of ones. A k-th decision variable $x_k = 1$ or $x_k = 0$ implies that a PMU is to or is not to be placed at one of the ends of a l_k transmission line, respectively. Note in (5) that the constraint $Ax \succeq \mathbf{1}$ ensures that every bus voltage becomes observable via measurement and/or estimation when placing the PMUs.

III. Load-Generation Disturbance Mitigation

A. Load-Generation Balance Calculation

A feasible solution of (5) ensures that all positive-sequence bus voltages, $\tilde{V}_j$ ($j = 1, \ldots, N$), and the currents leaving a bus, $\tilde{I}_{k,j}$ ($k = 1, \ldots, M$), become available at

a phasor data concentrator facility by direct measurement and/or estimation, see Section II-A and -B.

Therefore, it is feasible to calculate the net current injected at each bus b_j by application of Kirchoff's current law:[3]

$$\tilde{I}_j(\tau_s) = \sum_{\forall k: b_j \in \mathcal{L}_k} \tilde{I}_{k,j}(\tau_s)\,. \tag{6}$$

Indeed, one can obtain positive-sequence active power with:

$$P_j(\tau_s) = \mathtt{Re}\left(\tilde{V}_j(\tau_s)\tilde{I}_j^*(\tau_s)\right),\ \forall j\,. \tag{7}$$

Here, $\tau_s \in [t_s, t_{s+1})$ is introduced to indicate that PMU-processed phasors are stamped at a particular time $t = t_s$ ($s = 1, \ldots$) and are held constant until $t = t_{s+1}$, i.e., when a new measurement is processed. We consider a common phasor production period $T = t_{s+1} - t_s$ in all PMUs throughout a network to simplify the exposition.

B. Load-Generation Disturbance Estimation

Significant changes of a calculated $P_j(\tau_s)$ with respect to $P_j(\tau_{s-1})$ is indicative that a considerable amount of load-generation imbalance might have occurred at bus b_j during $t \in (t_{s-1}, t_s]$.[4] Here, load-generation disturbances, $\Delta p_j(t)$, at bus b_j are estimated dynamically with the wash-out filter:

$$\frac{d}{dt}p_j(t) = -\frac{1}{\tau_p}\left(p_j(t) - p_j^*(t)\right) \tag{8}$$

$$\Delta p_j(t) = p_j^*(t) - p_j(t) \tag{9}$$

where $p_j^*(t) = P_j(\tau_s)$ of (7) for $t \in [t_s + t_d, t_{s+1} + t_d)$. A time delay, t_d, models phasor processing times and communication latency.[5] Specifically, a $t \in [t_s + t_d, t_{s+1} + t_d)$ models the instant at which a command arrives to a converter asset given that the disturbance occurred at $t \in [t_s, t_{s+1})$. Note that (8) and (9) capture only fluctuations of a dynamic variable while removing steady-state offsets [19, p. 339].

The operational rationale of the filter is illustrated in Fig. 3. It shows that calculated power, $P(\tau_s)$, is applied to (8) and (9) in a delayed manner with $p_j^*(t)$ for $t \in [t_s + t_d, t_{s+1} + t_d)$. Sudden disturbances $\Delta p_j(t)$, e.g., at a particular bus, b_j, are estimated by subtracting, $p_j^*(t)$, from its first-order filtered version, $p_j(t)$. Note in Fig. 3 for $t > t_s + t_d$ that $\Delta p_j(t) \to 0$ as $t \to \infty$ and the convergence speed depends on the time constant $\tau_p > 0$ of (8). This convergence behavior is useful because conventional generation can compensate for the disturbance in a progressive manner.

C. Load-Generation Disturbance Mitigation

To avoid large frequency deviations as result of large load-generation imbalances and relatively slow acting governors, ultrafast responsive assets—e.g., EBS, WPP, SPP, and VFD-driven pumping stations—can be deployed [9]. That is, by adjusting their set points based on the estimated magnitude of load-generation imbalance as explained in Section III-B.

[3]Although it is possible to process $\tilde{I}_j$ from direct measurements, we do not consider this because it might imply handling several current sensors as a result of multiple generators and loads connected to a bus.

[4]Failure of instrumentation and/or the PMU itself could erroneously indicate power imbalances, but these are not considered in this paper.

[5]The time delay, t_d, can be a fraction of a second, e.g., $t_d = 0.5\,\mathrm{s}$.

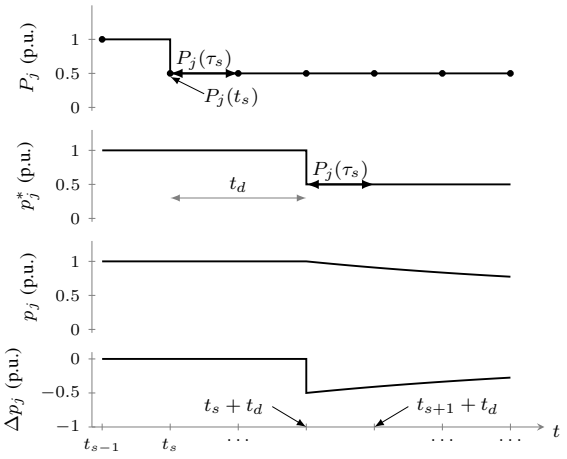

Fig. 3. Illustration of load-generation disturbance detection dynamics.

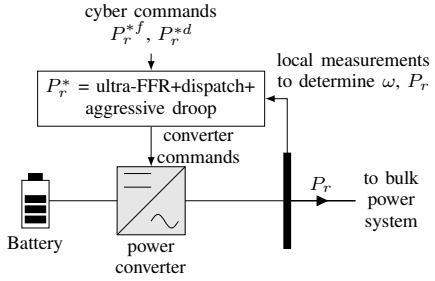

Fig. 4. Notional power converter with ultra-FFR, dispatchable, and aggressive-droop control commands. The picture can be expanded to subsystems powered by wind and solar in lieu of a battery.

To this end, let the estimated load-generation power imbalance in a grid be:

$$\Delta P(t) = \Delta p_\kappa(t) \tag{10}$$

with $\kappa = \mathrm{argmax}_{j \in \mathcal{J}}\{|\Delta p_j(t)|\}$ the bus index with the source of imbalance. This is determined at a data concentrator center using (9) $\forall j \in \mathcal{J}$. The set $\mathcal{J}$ models all bus indexes to which ultra-FFR assets are not attached. Also, let γ_r, $r = 1, 2, \ldots, R$, an ultra-FFR participation factor pertaining an r-th ultra-FFR asset that satisfies $\sum_r \gamma_r = 1$ with $\gamma_r \geq 0$. Then, the ultra-FFR power command an r-th asset must modulate is:

$$P_r^{*f}(t) = -\gamma_r \Delta P(t) \tag{11}$$

which is part of its net power command:

$$P_r^*(t) = P_r^{*f}(t) + P_r^{*d}(t) + P_r^{*\omega}(t)\,. \tag{12}$$

Here, $P_r^{*d}(t)$ is a dispatchable power command and $P_r^{*\omega}(t)$ is a frequency-sensitive power command. The total command, $P_r^*(t)$, can be followed by its actual version, $P_r(t)$, as long as this does not violate the physical limits of the BES, for example. Note in (12) that typically $P_r^{*d}(t) = 0$ in battery storage systems so they are not discharged unnecessarily during quasi-steady-state operation. Figure 4 shows a high-level illustration of the considered power commands and converter control. A similar control strategy can be applied to wind and solar assets as long as they are scheduled for this purpose.

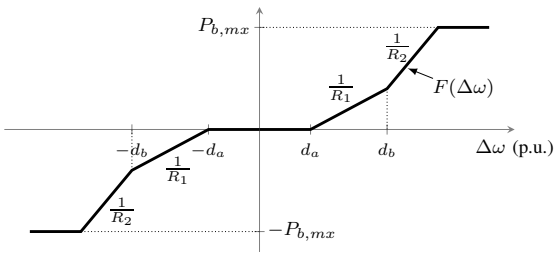

Fig. 5. Graphical definition of $F : \mathbb{R} \mapsto \mathbb{R}$ to provide aggressive droop.

D. Aggressive Frequency Droop

At least two problems arise when resorting to the command, $P_r^{*f}(t)$, to mitigate a load-generation disturbance, viz., vulnerabilities to communications failures and cyberattacks. In case of communications failures, $P_r^{*f}(t)$ might not respond if a disturbance occurs during such conditions. On the other hand, cyberattackers can stealthily introduce undesirable commands via $P_r^{*f}(t)$ and $P_r^{*d}(t)$, which can have a deleterious impacts on the power system frequency [11].

A possible counter measure to these problems is to furnish the system with local controls sensitive to frequency deviations $\Delta\omega = \omega^* - \omega$ from a nominal ω^* using the command:[6]

$$P_r^{*\omega}(t) = F(\Delta\omega) \tag{13}$$

with $F : \mathbb{R} \mapsto \mathbb{R}$ defined with two different slopes, as illustrated in Fig. 5. There, the power command, $P_r^{*\omega}(t)$, is zero when the frequency is within a predefined deadband, e.g., $d_a = 26$ mHz. If the frequency deviation falls below or above the deadband, the power converter can locally generate a power command that is proportional to the frequency deviation. This could occur because the ultra-FFR communications system is down or because of stealthy false data injection [11].[7] Depending on the strength of the deviation, two slopes are considered to provide both gentle (e.g., R_1 p.u. for $\Delta\omega \in [d_a, d_b]$) and aggressive (e.g., R_2 for $\Delta\omega > d_b$) frequency droop.

IV. Case Studies

We illustrate the contributions of this paper via simulations of a modified IEEE 39-bus test system which is shown in Fig. 6. The modifications are as follows: (i) The synchronous machines that were originally connected to buses B36 and B38 were displaced by equal-rating WPP and SPP, hence displacing 2.64 s and 3.45 s of inertia (in the 1000-MVA system base); (ii) A power converter interfacing a 800-MW BES subsystem is placed on bus B8. The power to be injected by the BES as well as the WPP is commanded by a PMU data concentrator facility, as explained in Sections III-B and III-C. They are equipped with aggressive droop control to counteract communications problems, as explained in Section III-D.

The PMU data concentrator is assumed to be within the geographic area of the test power system shown in Fig. 6. The PMUs are placed optimally, as described in Section II-B, so that all network voltages and currents are observable for power flow calculation purposes. The PMU locations are depicted in Fig. 6, which also shows graphically the solution to the optimization problem that is formulated in (4). A feasible solution for the considered power system is obtained via the `mpprog` function in MATLAB 2018a [20]. The modified IEEE 39-bus power system, which relies on [21], is simulated in Simulink Simscape Power Systems.

The system parameters to estimate the load-generation disturbance as explained in Section III-B are $\tau_p = 100$ s, $T = t_{s+1} - t_s = 1/30$ s, and $t_d = 0.5$ s. The time delay, t_d, modeling processing times and communications latency, is relatively large, but it can be considerably reduced in the future. The ultra-FFR participation factors in Section III-C for the BES and the WPP are $\gamma_1 = 0.9$ and $\gamma_2 = 0.1$, respectively. The SPP is insensitive to frequency transients; hence, the impact of the SPP is limited to the displacement of some synchronous inertia. The parameters of the aggressive droop function in Section III-D are $R_1 = 0.05$ p.u., $R_2 = 0.001$ p.u., $d_a = 4.3 \cdot 10^{-4}$ p.u., and $d_b = 0.001$ p.u. These parameters are judicious choices to illustrate the method; they were not rigorously determined.

Three case studies are conducted to illustrate the operational principle of ultra-FFR and the aggressive-droop strategy. In the two first case studies, the disturbance to the system is the disconnection of generator G2, which is tied to bus B31, as shown in Fig. 6. At disconnection of G2, it is injecting 765.6 MW and 305.9 Mvar; the cause of the disconnection could be an emergency shutdown. The third case study considers a hypothetical cyber intrusion in the PMU concentrator as to broadcast a false ultra-FFR request of 500 MW for 10 s. Case studies considering load disconnections are not shown because of space limitations.

For comparison, we introduce a reference case study. Figure 7 illustrates the system frequency response when G2 disconnects at $t = 20$ s and ultra-FFR and aggressive-droop strategies are inactive. Figure 7 illustrates the speed (or frequency, f, in p.u.) response of the rotor of each Gk ($k = 1, 3, 4, 5, 6, 8, 10$) machine. The short-lived transients right after $t = 20$ s are rotor oscillations, which might be insignificant in the context of this paper. The reference speed of each generator $\omega_k^* = f^* = 1$ p.u. and the UFLS threshold is $\underline{f} = 0.9917$ p.u. Note in Fig. 7 that the speed of the rotors can be as low as $f^a = 0.9945$ p.u. The UFLS risk margin, explained in the Introduction, is $\Delta f_a = f^a - \underline{f} = 0.0028$ p.u. For informational purposes, the rotor inertia of G2 is 3.03 s (in the 1,000-MVA system base); hence, this frequency response has an additional reduction in inertia.

A. Case Study I

Figure 8 illustrates the response of the system when only ultra-FFR is active. The detected disturbance at $t = 20$ s is $\Delta P = -0.7618$ p.u. This is indicative that the system has lost 761.8 MW which is relatively close to the generation of G2 before its outage, i.e., 765.6 MW. The lowest rotor speed in the system (or frequency nadir) is $f^a = 0.9986$ p.u., which yields $\Delta f^a = 0.0069$ p.u. Notably, the ultra-FFR method yields an absolute UFLS risk improvement of 0.0041 p.u. (or 0.246 Hz) with respect to the reference case. Note in Fig. 8 at $t = 20.5$ s that the BES and WPP are commanded

[6] In this paper, ω is the weighted average of the rotor speed of each synchronous machine [16].

[7] We assume that cybersecurity layers might be insufficient to protect the systems from cyber intruders.

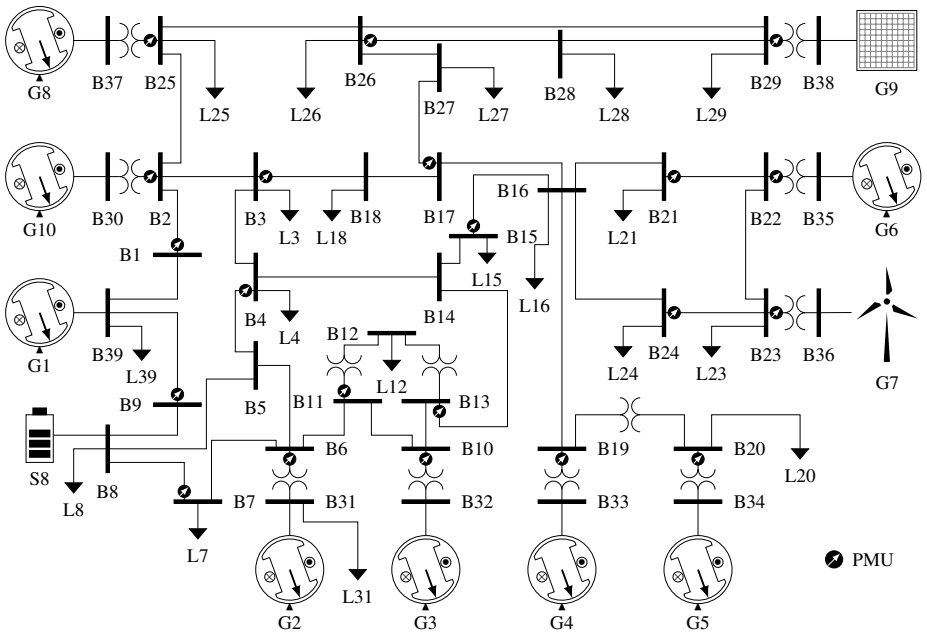

Fig. 6. Modified IEEE 39-bus power system with optimally placed PMUs.

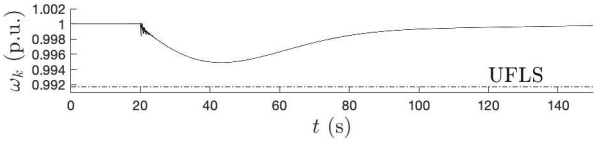

Fig. 7. System response during outage of G2 when ultra-FFR and aggressive droop support are inactive.

to supply additional $P_1^{*f} = -\gamma_1 \Delta P = 0.686\,\text{p.u.}$ and $P_2^{*f} = -\gamma_2 \Delta P = 0.0762\,\text{p.u.}$, respectively. The WPP does not sustain the command P_1^{*f} because it modulates over a maximum-power point-tracking set point, hence the extra power extraction is short lived, see [9]. If the WPP were operating sub-optimally, it is possible to extract extra power in a sustained manner. The BES can follow the requested command, P_2^{*f}, only if there is enough battery capacity to inject or absorb power.

B. Case Study II

Figure 9 illustrates the response of the system when only aggressive droop is active. The lowest rotor speed (or frequency nadir) is $f^a = 0.9982$ p.u., which signifies $\Delta f^a = 0.0065\,\text{p.u.}$ Notably, the aggressive-droop method yields an absolute UFLS risk improvement of 0.0037 p.u. (or 0.222 Hz) with respect to the reference case and slightly less than that of Case Study I. Note at $t = 20\,\text{s}$ that the BES and WPP modulate their power injections depending on the frequency deviation level following the function illustrated in Fig. 5. The maximum power that the WPP can modulate for aggressive-droop is constrained to $0.1\,\text{p.u.}$ for comparison purposes with ultra-FFR.

C. Case Study III

Figure 10 illustrates the response of the system when ultra-FFR and aggressive-droop are active and there is a cyberattack. The attack introduces false data at the PMU concentrator facility to mimic a 500-MW loss of power

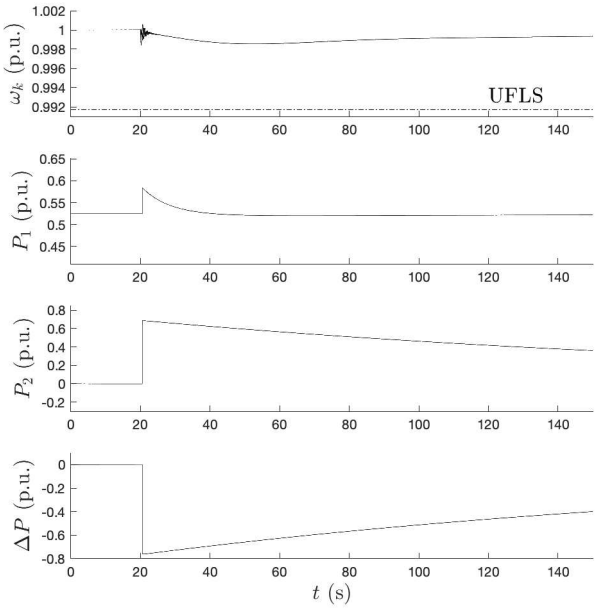

Fig. 8. System response during outage of G2 when ultra-FFR is active, but aggressive droop support is inactive.

generation. The cyberattack takes place at $t = 20\,\text{s}$, which is detected and cleared after $10\,\text{s}$ of the intrusion by cyber-security systems. During the attack, the BES and the WPP are both commanded to inject 500 MW to counteract this "virtual" event. Because unnecessary power is injected into the grid, the average speed of the rotors reaches a maximum (or frequency zenith) of 1.0014 p.u. Hence, the aggressive droop strategy activated to generate a power droop command that counteracts the physical impact of the cyberattack. After the cyberattack is removed, the system recovers to its normal operating condition.

V. Conclusion

This paper elaborated on the technical aspects of an ultra-FFR method using strategically located PMUs. The control

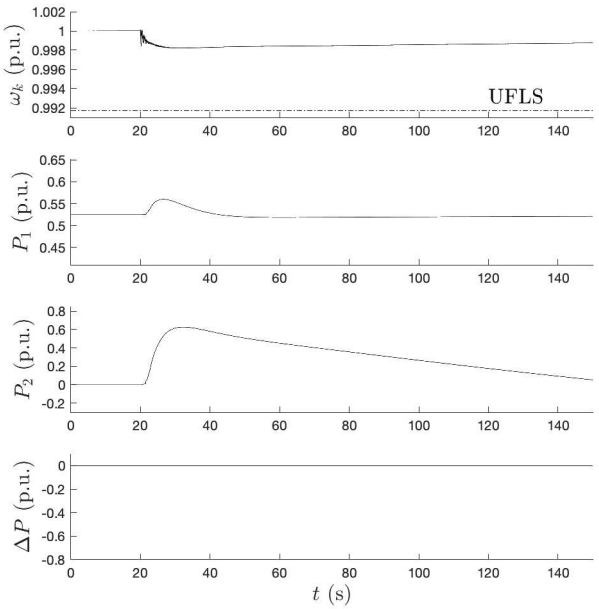

Fig. 9. System response during outage of G2 when ultra-FFR is inactive, but aggressive droop support is active.

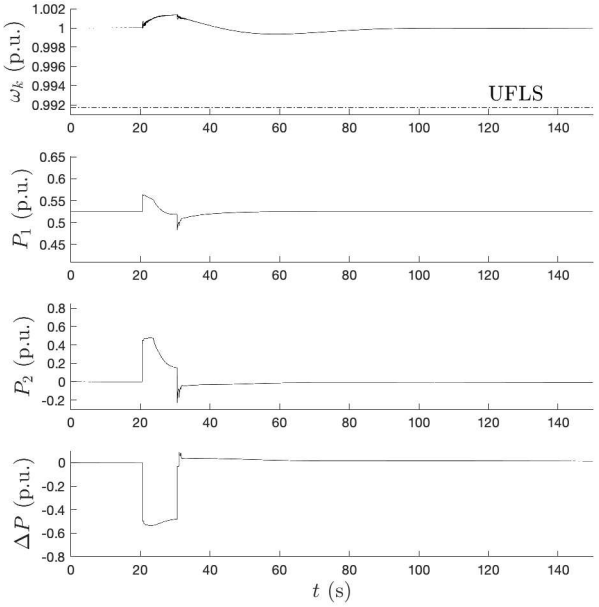

Fig. 10. System response during a cyberattack when ultra-FFR and aggressive droop support are active.

method reduces the risk associated with the activation of UFLS in systems with significant penetrations of converter-based generation. In case of communications unavailability, an aggressive-droop control strategy has been introduced to compensate for the load-generation imbalances in a relatively fast manner. The aggressive droop control is also suitable to diminish the impact of cyberattacks that can negatively manipulate ultra-FFR assets. Technological and/or physical constraints to achieve close-to-instantaneous compensation to disturbances are, for example, PMU information processing times and communications latency.

In this paper, the economic aspects of ultra-FFR participation factors were not considered. Also, this paper did not elaborate on the necessary headroom of converter-based assets to release or absorb power as well as to regulate voltages. Further, the selection of control parameters still needs to be rigorously addressed. These topics represent future research directions.

VI. Acknowledgements

The authors thank Charlton Clark and Jian Fu of the U.S. DOE's WETO for their continuous support of this project.

References

[1] NERC, "State of reliability 2018," North American Electric Reliability Corporation, Atlanta, GA, Tech. Rep., Jun. 2018.

[2] Q. Hong *et al.*, "Fast frequency response for effective frequency control in power systems with low inertia," *The J. of Eng.*, vol. 3, no. 16, pp. 1696–1702, Apr. 2018.

[3] N. Shams, P. Wall, and V. Terzija, "Active power imbalance detection, size and location estimation using limited PMU measurements," *IEEE Trans. Power Syst.*, vol. 34, no. 2, pp. 1362–1372, Mar. 2019.

[4] NERC, "State of reliability 2019," North American Electric Reliability Corporation, Atlanta, GA, Tech. Rep., Jun. 2019.

[5] M. Kayikçi and J. V. Milanović, "Dynamic contribution of DFIG-based wind plants to system frequency disturbances," *IEEE Trans. Power Syst.*, vol. 24, no. 2, pp. 859–867, May 2009.

[6] R. Eriksson, N. Modig, and K. Elkington, "Synthetic inertia versus fast frequency response: a definition," *IET Renewable Power Generation*, vol. 15, no. 5, pp. 507–514, Sep. 2018.

[7] Y. Bian *et al.*, "Demand side contributions for system inertia in the GB power system," *IEEE Trans. Power Syst.*, vol. 33, no. 4, pp. 3521–3530, Jul. 2018.

[8] A. Delavari and I. Kamwa, "Improved optimal decentralized load modulation for power system primary frequency regulation," *IEEE Trans. Power Syst.*, vol. 33, no. 1, pp. 1013–1025, Jan. 2018.

[9] H. N. Villegas Pico, V. Gevorgian, P. Koralewicz, and R. Wallen, "Role of motor loads and battery energy storage for active power controls by wind power," in *Proc. 17th Int. Workshop Large-Scale Integration of Wind Power into Power Syst. as well as Transmission Networks for Offshore Wind Power Plants*, Stockholm, Sweden, Oct. 2018.

[10] H. X. Zhang, F. Shi, Y. T. Liu, and V. Terzija, "Adaptive on-line disturbance location considering anisotropy of frequency propagation speeds," *IEEE Trans. Power Syst.*, vol. 31, no. 2, pp. 931–941, Mar. 2016.

[11] A. Ashok, M. Govindarasu, and V. Ajjarapu, "Online detection of stealthy false data injection attacks in power system state estimation," *IEEE Trans. Smart Grid*, vol. 9, no. 3, pp. 1636–1646, May 2018.

[12] K. Emami, T. Fernando, H. Ho-Ching Iu, H. Trinh, and K. P. Wong, "Particle filter approach to dynamic state estimation of generators in power systems," *IEEE Trans. Power Syst.*, vol. 30, no. 5, pp. 2665–2675, Sep. 2015.

[13] J. Zhao, G. Zhang, K. Das, G. N. Korres, N. M. Manousakis, A. K. Sinha, and Z. He, "Power system real-time monitoring by using PMU-based robust state estimation method," *IEEE Trans. Power Syst.*, vol. 7, no. 1, pp. 300–309, Jan. 2016.

[14] E. Ghahremani and I. Kamwa, "Local and wide-area PMU-based decentralized dynamic state estimation in multi-machine power systems," *IEEE Trans. Power Syst.*, vol. 31, no. 1, pp. 547–562, Jan. 2016.

[15] Power System Relaying Committee, *IEEE Guide for Synchronization, Calibration, Testing, and Installation of Phasor Measurement Units (PMUs) for Power System Protection and Control*, IEEE Power and Energy Society Std. IEEE Std C37.242^{TM}-2013, Feb. 2013.

[16] P. W. Sauer and M. A. Pai, *Power System Dynamics and Stability*. Champaign, Illinois: Stipes Publishing L.L.C., 2006.

[17] J. Kleinberg and E. Tardos, *Algorithm Design*, 1st ed. Boston, MA: Pearson, 2006.

[18] M. Bagajewicz, A. Fuxman, and A. Uribe, "Instrumentation network design and upgrade for process monitoring and fault detection," *AIChE J.*, vol. 50, no. 8, pp. 1870–1880, Jul. 2004.

[19] P. M. Anderson and A. A. Fouad, *Power System Control and Stability*, 2nd ed., ser. IEEE Press Power Engineering Series. John Wiley & Sons, 2003.

[20] (2018) MATLAB R2018a. The MathWorks Inc. Natick, MA. [Online]. Available: http://www.mathworks.com

[21] A. Moeini, I. Kamwa, P. Brunelle, and G. Sybille, "Open data IEEE test systems implemented in SimpowerSystems for education and research in power grid dynamics and control," in *50th Int. Universities Power Eng. Conf.*, Stoke on Trent, UK, Sep. 2015.